IEEE Access
Multidisciplinary ⋮ Rapid Review ⋮ Open Access Journal

Received 25 February 2023, accepted 19 March 2023, date of publication 27 March 2023, date of current version 12 April 2023.

Digital Object Identifier 10.1109/ACCESS.2023.3262463

RESEARCH ARTICLE

Design of a Dual-Polarization All-Metal Vivaldi Array Antenna Using a Metal 3D Printing Method for High-Power Jamming Systems

SUNGSIK OHM[1], EUNJUNG KANG[1], TAE HEUNG LIM[2], AND HOSUNG CHOO[1], (Senior Member, IEEE)

[1]Department of Electronic and Electrical Engineering, Hongik University, Seoul 04066, South Korea
[2]Agency for Defense Development, Daejeon 34186, South Korea

Corresponding author: Hosung Choo (hschoo@hongik.ac.kr)

This work was supported by Agency for Defense Development - Grant funded by Defense Acquisition Program Administration (UI210013YD).

ABSTRACT This paper proposes an all-metal Vivaldi array antenna with a wide-angle impedance matching (WAIM) layer for high-power jamming systems. To reduce fabrication complexity and time, the proposed array antenna is manufactured using a metal 3D printing method. The Vivaldi unit cell, composed of a radiating flare part and an inner cavity, is extended into an 8×8 array with a $\pm 45°$ slant configuration. To further enhance the beam steering angle, the WAIM layer is placed on top of the proposed array antenna. The performances of the proposed array antenna, such as its active reflection coefficients (ARCs), gains, and array radiation patterns, are investigated in a full anechoic chamber. At a steering angle of ($\theta_0 = 45°$, $\phi_0 = 25°$), the measured and simulated average ARCs of the center element (Port 36) with the WAIM layer are -13.2 dB and -18.5 dB, respectively. At 4 GHz, the measured and simulated boresight gains of the proposed array antenna are 19 dBi and 20.6 dBi, respectively. In addition, the measured and simulated boresight gains for the ($\theta_0 = 45°$, $\phi_0 = 0°$) steering angle in the *zx*-plane are 18 dBi and 21 dBi, respectively. In the *zy*-plane, boresight gains for the ($\theta_0 = 45°$, $\phi_0 = 0°$) steering angle are 19.3 dBi by measurement and 19.1 dBi by simulation. These results demonstrate that the proposed array antenna is suitable for high-power jamming systems because stable boresight gains are observed even at wide steering angles without unwanted grating lobes.

INDEX TERMS 3D printing, all-metal Vivaldi array, high-power jamming systems, unit cell array, wide angle impedance matching.

I. INTRODUCTION

In recent electronic warfare, high-power jamming systems have often been used to disrupt enemy radio frequency (RF) radar systems in vehicles, ships, and aircraft by transmitting broadband interference RF waves [1], [2], [3], [4]. These high-power jamming systems require phase array antennas with broadband characteristics, since the various target RF devices typically operate in multiple frequency bands. In previous studies, efforts have been made to improve the operating frequency bandwidth of antennas by applying various structures, such as a horn antenna integrated with a substrate board [5], [6], spiral antennas based on a hybrid backed-cavity [7], [8], and a microstrip patch antenna with an L-shaped indirect feed [9], [10]. Although these antennas can achieve the broadband characteristics, the element antenna size is too large to extend to an array antenna. To solve this problem, many studies have attempted to make the antenna elements thinner and smaller, such as printed LPDAs fed by a coplanar waveguide [11], [12] printed Vivaldi antennas using a tapered slot edge or cavity structure [13], [14], and bow-tie slot antennas with cavity-backed design [15], [16]. However, these techniques are still difficult to be applied to dual-polarization high-power jamming systems, which require a much higher level of fabrication complexity [17], [18]. In addition, these antennas are usually fabricated with dielectric substrates that exhibit low durability characteristics under high-power operations. Recently,

The associate editor coordinating the review of this manuscript and approving it for publication was Fulvio Schettino.

all-metal Vivaldi array antennas, which can be employed in dual-polarization high-power jammer systems, have been introduced [19]. The metal bodies of Vivaldi antennas are typically fabricated using casting or laser-cutting methods. However, these methods encounter difficulties in precisely machining the delicate curved surfaces required to prevent arcing under high-power operations. In addition, these methods require the fabrication of each antenna part separately, where the final design is completed by assembling each part, thus increasing the manufacturing complexity and time.

In this paper, we propose an all-metal Vivaldi array antenna with a wide-angle impedance matching (WAIM) layer for high-power jamming systems. To reduce manufacturing complexity and time, the proposed array antenna is manufactured using a metal 3D printing method. Among the various available metal 3D printing techniques, the selective laser melting (SLM) method is used to fabricate the complicated volumetric structure of Vivaldi unit cells and the ground plate. The Vivaldi unit cell is composed of a radiating flare part and an inner cavity. The shapes of the radiating flares are adjusted to obtain high directivity with minimal pattern distortion in the boresight direction. Meanwhile, the inner cavity of the antenna has a significant impact on its impedance matching characteristics, thus enabling broadband operations. To enhance high-power durability, a rounded shape is adopted to the sharp parts of the Vivaldi unit cell to reduce the E-field distribution level and prevent arc flashes. The single Vivaldi unit cell is extended to an 8 × 8 array with a ±45° slant configuration, which achieves the maximum beam steering angle. Moreover, to further enhance the beam steering angle, the WAIM layer is placed on top of the proposed array antenna, thus improving the active reflection coefficients (ARCs) and beam steering performance in the operating frequency band. The performances of the proposed array antenna, such as the ARCs, gains, and array radiation patterns, are investigated using the CST studio suite [20], the ANSYS high-frequency structure simulator (HFSS) [21], [22] and measurements. The results demonstrate that an array antenna fabricated using the metal 3D printing method has the broadband and wide beam steering characteristics, which is suitable for application in high-power jamming systems in the operating frequency range of 2 GHz to 6 GHz.

II. VIVALDI UNIT CELL DESIGN FOR METAL 3D PRINTING METHOD

Figs. 1(a) and 1(b) illustrate the front and isometric views of the proposed array element, which consists of radiating flares and an inner cavity. The radiating flares have an exponential curve that uses the equations of $f(z)$, expressed as follows:

$$f(z) = a \times e^{k(z-l_2)}, \tag{1}$$

$$k = \frac{1}{l_1}\left(\frac{w_1 - w_3}{2a} + 1\right), \tag{2}$$

where a is a function coefficient of the exponential curve. Furthermore, l_1 has a significant influence on directivity and w_1 determines the operating frequency band. The cavity is an

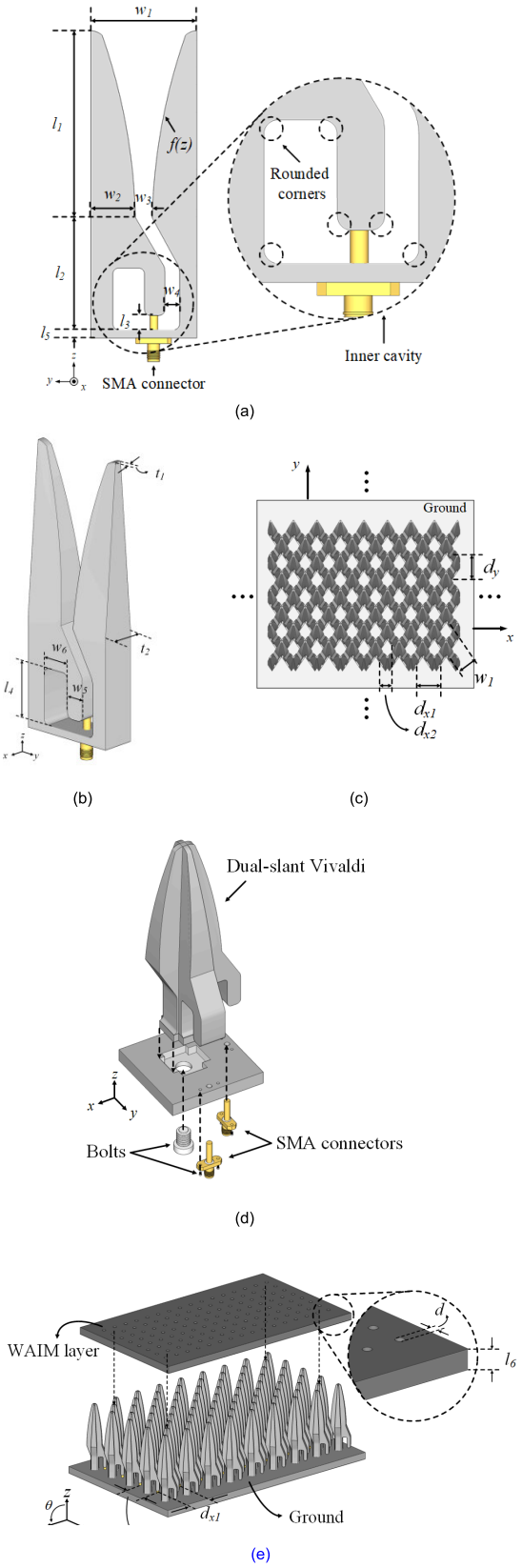

FIGURE 1. Geometry of the proposed array antenna. (a) Front view of the array element. (b) Isometric view of the array element. (c) The proposed array configuration. (d) Vivaldi unit cell for applying the metal 3D printing method. (e) The 8 × 8 array with the WAIM layer.

TABLE 1. Design parameters of the proposed array antenna.

Parameters	Optimized values
a	0.99
l_1	90 mm
l_2	30.5 mm
l_3	1.5 mm
l_4	15 mm
l_5	5 mm
l_6	1.53 mm
w_1	29.7 mm
w_2	13.7 mm
w_3	2.4 mm
w_4	1.6 mm
w_5	11 mm
w_6	10.8 mm
t_1	1.07 mm
t_2	4.5 mm
d_{x1}	42 mm
d_{x2}	21 mm
d_y	42 mm
d	2 mm

important structure for impedance matching characteristics. The bandwidth can be also enhanced by tuning the size of the $l_4 \times w_6$ rectangle constituting this structure, since the impedance matching characteristics can be improved by optimizing an electrical current path according to the size of the cavity in the operating frequency band. The total height (l_1+l_2) of the proposed antenna is 2.4λ (120.5 mm) at 6 GHz. In addition, rounded shapes are applied to the inner cavity to improve high-power durability by reducing the E-field distribution level at sharp corners to prevent an arc flash. Fig. 1(c) illustrates the array configuration of the proposed array antenna.

However, this array element cannot be used in planar arrays because its width ($w_1 = 0.6\lambda$) is larger than 0.5λ at 6 GHz, resulting in unwanted grating lobes. For implementing dual polarization, the array element is rotated ±45° based on its center and extended into the array antenna. In addition, an x-shift is applied to the array configuration to avoid grating lobes by reducing the array distance.

Fig. 1(d) presents the Vivaldi unit cell structure, which can be efficiently fabricated by a metal 3D printing method. Notably, adopting metal 3D printing reduces manufacturing costs, complexity, and time. The unit cell of the dual-slant Vivaldi structure is designed to be more suitable for metal 3D printing by combining the +45° and –45° slanted antennas into a single piece. Thus, the unit cell consisting of four radiating flares and two inner cavities can be made in a single process through metal 3D printing. The unit cell is fed by bolted SMA connectors. Fig. 1(e) presents the fully assembled 8 × 8 array with the WAIM layer. The spacing between the array elements along the x- and y-axis are d_{x1} and d_y, respectively. The array distance used for the x-shift is d_{x2}, which is half that of d_{x1}. To improve beam steering performance, the WAIM layer is designed using a TLY-5 ($\varepsilon_r = 2.2$, $\tan\delta = 0.0009$) substrate with thickness l_6, wherein circular holes of diameter d are perforated to obtain the required permittivity. This layer can improve the ARCs by compensating for the offset susceptance component during beam steering

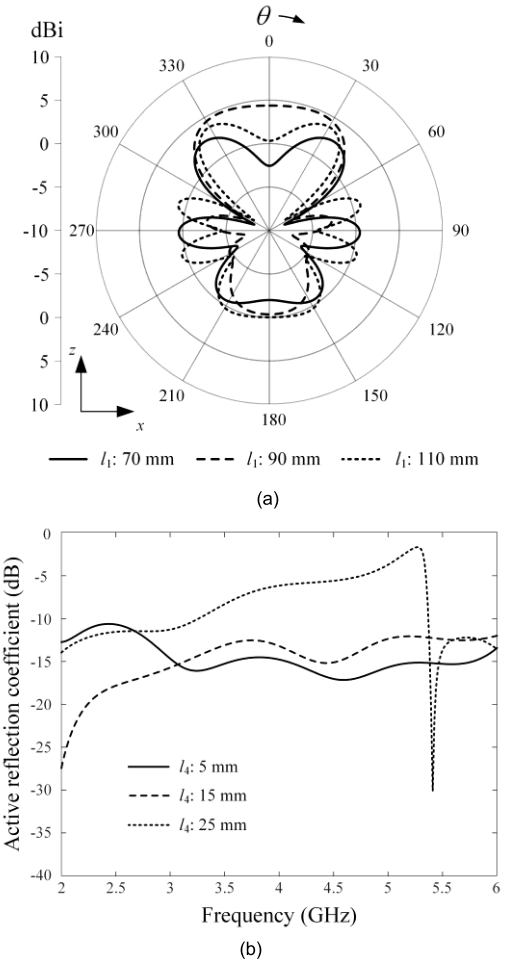

FIGURE 2. Parametric studies for the radiating flares and cavity. (a) 2D radiation patterns according to radiating flares. (b) Active reflection coefficients according to cavity.

[23], [24], [25]. The optimized design parameters are listed in Table 1.

Fig. 2(a) shows the parametric study of the shape of the radiating flares. To confirm the directivity at the boresight, we observe the 2D radiation patterns when increasing the flare length of l_1 from 70 mm to 110 mm at a center frequency of 4 GHz. When the flare length l_1 is 90 mm, the maximum directivity is 4.72 dBi at the boresight direction and it is confirmed that the flare length l_1 can affect the radiation pattern, especially at the boresight. Fig. 2(b) presents the parametric study for the size of the cavity. We confirm the ARCs according to the cavity height l_4 from 5 mm to 25 mm using a linear periodic structure. The results show that ARCs are less than −10 dB in the operating frequency when the cavity height of l_4 is 15 mm. This is because the cavity height can tune the total current path, which enables the operation of the antenna in the frequency band of 2 GHz to 6 GHz.

In general, during high-power operations, arc flashes occur frequently at the sharp edges of metal Vivaldi structures. To overcome this problem, we apply rounded shapes to the tips of the radiating flares and the corners of the cavity. Fig. 3 shows the E-field distribution values with and without

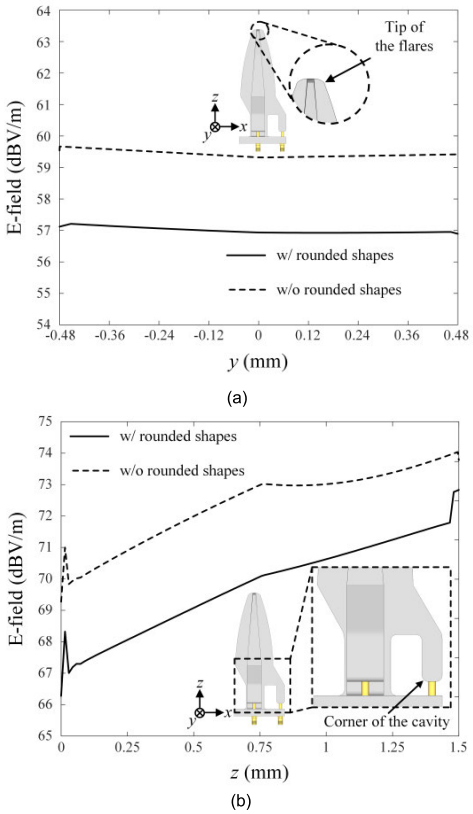

FIGURE 3. E-field distributions depending on the rounded shapes. (a) With and without rounded tips. (b) With and without rounded cavities.

rounded shapes in the Vivaldi unit cell. When the origin ($x = 0$, $y = 0$, $z = 0$) is the center of the ground plate's top surface, the coordinates of the tip center are ($x = 0$, $y = 0$, $z = 120$ mm). In the Fig. 3(a), we observe the E-field distribution slightly above the tip at a center frequency of 4 GHz. The average E-field distribution values with and without the rounded shapes along the y-axis above the tip ($x = 1.2$ mm, -0.48 mm $< y < 0.48$ mm, $z = 120.5$ mm) are 56.9 dBV/m and 59.4 dBV/m, respectively. These results indicate that the average E-field distribution value decreases by 2.5 dB when rounded shapes are applied to the tip of the Vivaldi unit cell. Fig. 3(b) presents the E-field distributions of the ground between the corners of the cavity, indicated by arrow ($x = 4.85$ mm, $y = 2.25$ mm, $0 < z < 1.5$ mm). These results also show that applying rounded shapes decreases the average E-field distribution values of the cavity by 2.6 dB from 72.4 dBV/m to 69.8 dBV/m. Therefore, both results demonstrate that rounded shapes can reduce the concentration of E-field distribution, which make the proposed array antenna more suitable for high-power jamming systems, as it reduces the probability of the occurrence of arc flashes.

III. FABRICATION USING METAL 3D PRINTING METHOD AND MEASUREMENT

A. FABRICATION USING METAL 3D PRINTING METHOD

Fig. 4 presents photographs of the array antenna fabricated using the SLM metal 3D printing method, which melts and

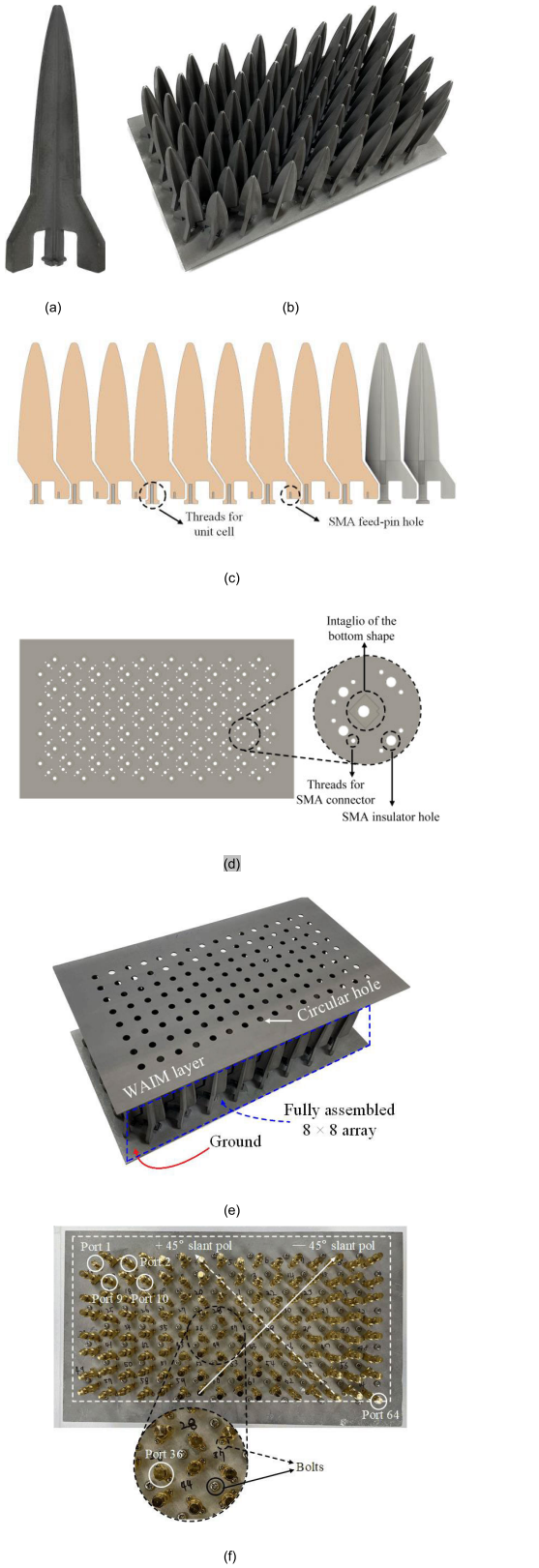

FIGURE 4. Photographs of the fabricated array antenna. (a) Vivaldi unit cell structure. (b) The fully assembled 8 × 8 array. (c) Side view of the 3D CAD cross section of metal Vivaldi arrays. (d) Top view of the 3D CAD of ground. (e) The fabricated 8 × 8 array with the WAIM layer. (f) The bottom view of the fabricated array antenna.

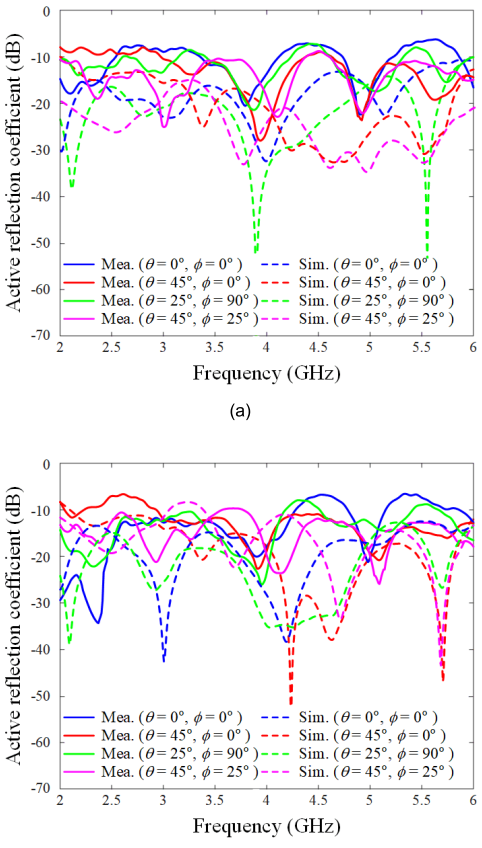

FIGURE 5. Measured and simulated ARCs of the proposed array antenna. (a) With WAIM layer. (b) Without WAIM layer.

fuses metallic powder with a high-power laser to create a high-density metal structure [26]. We use aluminum as the metallic powder because it is lightweight, inexpensive, and durable at high temperatures. The SLM metal 3D printing method generally uses metal powder with a particle size of 20 μm to 50 μm and a laser beam with a diameter of 20 μm to 30 μm. Therefore, the high resolution SLM method can easily fabricate the proposed unit cell and ground, thus simplifying the assembly process of the unit cells and SMA connectors. Fig. 4(b) represents the fully assembled 8 × 8 array that can achieve dual-slant polarization. Fig. 4(b) represents the fully assembled 8 × 8 array that can achieve dual-slant polarization. The antenna is made of 128 array elements, which are equivalent to 77 Vivaldi unit cells from another perspective. Fig. 4(c) illustrates the cross-section of the 3D CAD, which contains threads and holes for the SMA feed-pin. Fig. 4(d) exhibits the 3D CAD of the ground plate, where intaglio shapes are added to facilitate the connection between the unit cells and the ground plate. Threads and holes are inserted to fasten the SMA connectors. Fig. 4(e) shows the fabricated 8 × 8 array with the WAIM layer placed on top of the array antenna to widen the beam steerable angle. The WAIM layer is fabricated using a perforated TLY-5 substrate with a thickness of 1.53 mm and a diameter of 2 mm for the circular holes. The Vivaldi unit cells, fed by SMA connectors, are bolted to the ground plate, as shown in Fig. 4(f). The white

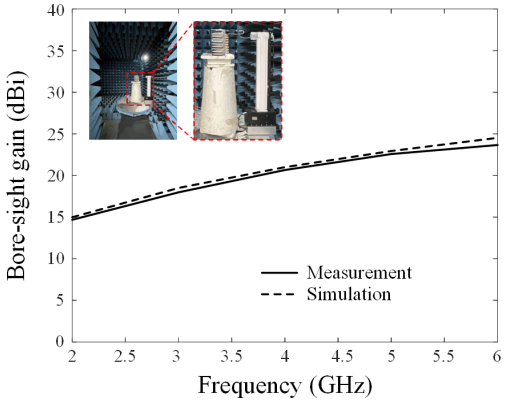

FIGURE 6. Measured and simulated boresight gains of the proposed array antenna.

TABLE 2. Antenna performances of the proposed antenna with some previous studies.

Plane	*zx*-plane				*zy*-plane			
θ_0	0°	15°	30°	45°	0°	15°	30°	45°
Mea. (dBi)	20	18.3	18.2	18	19.3	19.7	19.7	19.3
Sim. (dBi)	23.7	23.6	23	21	20.7	20.5	20	19.1

circles indicate the SMA ports numbered 1, 2, 9, 10, 36, and 64 (+45° slant-polarized elements).

B. MEASUREMENT RESULTS OF THE PROPOSED ARRAY ANTENNA

Fig. 5. shows the measured and simulated ARCs of the proposed array antenna, with and without the WAIM layer. To achieve the ARCs, the S-parameters of the array antenna should be measured first. When measuring the S-parameters, all ports, except for the two measuring ports, are terminated with 50-Ω loads. When steering at angles of θ_0 and ϕ_0, the ARCs of elements located in the mth row and the nth column are calculated using the measured S-parameters as follows [27], [28]:

$$\begin{aligned}\Gamma_i(\theta_0, \phi_0) &= \sum_{n=1}^{N/2}\sum_{m=1}^{N} S_{i,\, m+M(n-1)} \\ &\times (e^{-jk[(m-1)d_{x1}\sin\theta_0\cos\phi_0+(2n-2)d_y\sin\theta_0\sin\phi_0]} \\ &+ e^{-jk[d_{x2}+(m-1)d_{x1}\sin\theta_0\cos\phi_0+(2n-1)d_y\sin\theta_0\sin\phi_0]}), \quad (3)\end{aligned}$$

where d_{x1} and d_y are the array distances between adjacent elements in each x- and y-axis, respectively. Furthermore, d_{x2} is the x-shift distance, while M and N refer to the numbers of rows and columns, respectively, and k is a wave number. The blue, red, green, and magenta lines indicate the ARCs results of the center element (Port 36) at each steering angle (θ_0, ϕ_0) of (0°, 0°), (45°, 0°), (25°, 90°), and (45°, 25°). The solid lines indicate the measured ARCs, while the dashed lines represent the simulated ARCs. The measured and simulated

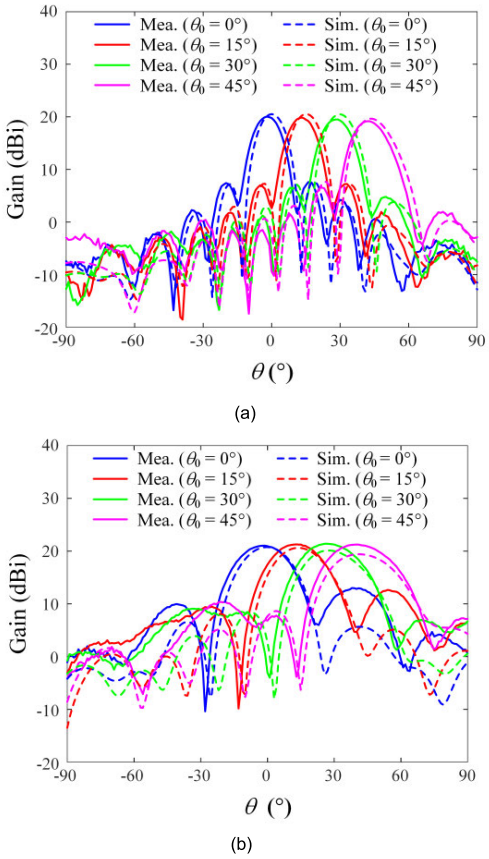

FIGURE 7. Array beam pattern for the proposed 8 × 8 array. (a) zx-plane. (b) zy-plane.

average ARCs at the steering angle (45°, 25°) of the center element (Port 36) with the WAIM layer are −13.2 dB and −18.5 dB, respectively. On the other hand, the average ARCs without the WAIM layer are −9.2 dB by measurement and −17 dB by simulation. It is confirmed that the measured ARCs with the WAIM layer are improved by an average of 4 dB. Finally, the active element patterns (AEPs) of the proposed array antenna are measured to confirm the beam steering performance, which is another essential array characteristic for high-power jamming systems. To measure the AEPs, each array element is successively excited, while all other ports are terminated with 50-Ω loads. The AEPs of the proposed array antenna are then obtained using equation (4), as follows [29], [30]:

$$G_{array}(\theta_0, \phi_0) = \frac{\sum_{n=1}^{N} w_n v_n(\theta_0, \phi_0)}{\sqrt{\sum_{n=1}^{N} |w_n|^2}}, \tag{4}$$

where w_n is a weighting vector for beam steering and v_n refers to a complex AEP vector of an n^{th} port. Fig. 6 shows the measured and simulated boresight gains of the proposed array antenna. At a center frequency of 4 GHz, the measured and simulated boresight gains are 19 dBi and 20.6 dBi, respectively. Notably, the measurements of the AEPs are carried out in a full anechoic chamber. Overall, the measurement results for the proposed 8 × 8 array with the WAIM layer are in good agreement with the simulated results.

Fig. 7 shows the array beam pattern for the proposed 8 × 8 array according to the steering angle θ_0 when ϕ_0 is fixed at 0°. To verify the beam steering performance at a center frequency of 4 GHz, the measured and simulated results in the zx- and zy-planes are compared. At the steering angle $\theta_0 = 0°$, the measured and simulated boresight gains of the zx-plane are 20 dBi and 23.7 dBi, respectively. Meanwhile, the boresight gains of the zy-plane are 20.7 dBi by measurement and 19.3 dBi by simulation. To investigate beam steering performance, we increase the steering angle θ_0 up to 45°, after which the measured and simulated boresight gains in the zx-plane are slightly decreased to 18 dBi and 21 dBi, respectively. In the zy-plane, the boresight gains are 19.3 dBi by measurement and 19.1 dBi by simulation. The beam steering results of the proposed array antenna for steering angles $\theta_0 = 0°$, 15°, 30°, and 45° are listed in Table 2. These results demonstrate that the proposed array antenna is suitable for use in high-power jamming systems because stable boresight gains without unwanted grating lobes are observed, even at wide steering angles.

IV. CONCLUSION

We proposed the all-metal Vivaldi array antenna with the WAIM layer for high-power jamming systems. The proposed array antenna was fabricated using the SLM metal 3D printing method to reduce fabrication complexity and time. The Vivaldi unit cell was composed of radiating flares and the inner cavity, and it was extended to the 8 × 8 array with a ±45° slant configuration. To further enhance the beam steering angle, the WAIM layer was placed on top of the proposed array antenna, which improved its ARCs by compensating for the offset susceptance component during beam steering. For the steering angle ($\theta_0 = 45°$, $\phi_0 = 25°$), the measured and simulated average ARCs of the center element (Port 36) with the WAIM layer were −13.2 dB and −18.5 dB, respectively. Furthermore, the measured and simulated boresight gains of the proposed array antenna at 4 GHz were 19 dBi and 20.6 dBi, respectively. For the ($\theta_0 = 45°$, $\phi_0 = 0°$) steering angle, the measured and simulated boresight gains in the *zx*-plane were 18 dBi and 21 dBi, respectively. Meanwhile, in the *zy*-plane, the boresight gains for the ($\theta_0 = 45°$, $\phi_0 = 0°$) steering angle were 19.3 dBi by measurement and 19.1 dBi by simulation. These results demonstrated that the proposed array antenna was suitable for high-power jamming systems due to its stable boresight gains without unwanted grating lobes.

REFERENCES

[1] Q. J. O. Tan and R. A. Romero, "Jamming-nulling transmit-adaptive radar against knowledge-based jammers in electronic warfare," *IEEE Access*, vol. 7, pp. 181899–181975, 2019.

[2] Y. Yang, K. Li, J. Li, H. Zhu, Y. Zhang, and K. Huang, "Low-cost, high-power jamming transmitter based on magnetron," *IEEE Trans. Electron Devices*, vol. 67, no. 7, pp. 2912–2918, Jul. 2020.

[3] Z. Li, B. Hu, and Z. Yang, "Co-design of distributed event-triggered controller for string stability of vehicle platooning under periodic jamming attacks," *IEEE Trans. Veh. Technol.*, vol. 70, no. 12, pp. 13115–13128, Dec. 2021.

[4] S.-H. Lim, S. Han, J. Lee, Y. Eun, and J.-W. Choi, "Decoy signal based strategic beamforming against high-power reactive jamming," *IEEE Trans. Veh. Technol.*, vol. 67, no. 10, pp. 10054–10058, Oct. 2018.
[5] Y. Cai, Y. Zhang, Z. Qian, W. Cao, and L. Wang, "Design of compact air-vias-perforated SIW horn antenna with partially detached broad walls," *IEEE Trans. Antennas Propag.*, vol. 64, no. 6, pp. 2100–2107, Jun. 2016.
[6] S. Lee and J. Choi, "All-textile corrugated ground SIW horn antenna for millimeter-wave WBAN applications," *J. Electromagn. Eng. Sci.*, vol. 19, no. 4, pp. 221–226, Oct. 2019.
[7] C. Liu, Y. Lu, C. Du, J. Cui, and X. Shen, "The broadband spiral antenna design based on hybrid backed-cavity," *IEEE Trans. Antennas Propag.*, vol. 58, no. 6, pp. 1876–1882, Jun. 2010.
[8] P. H. Rao, M. Sreenivasan, and L. Naragani, "Dual band planar spiral feed backed by a stepped ground plane cavity for satellite boresight reference antenna applications," *IEEE Trans. Antennas Propag.*, vol. 57, no. 12, pp. 3752–3756, Dec. 2009.
[9] D. Jang, S. Yoo, and H. Choo, "Design of patch antenna with polarization control module to achieve broad 3-dB gain bandwidth over entire AR range," *Microw. Opt. Technol. Lett.*, vol. 62, no. 7, pp. 2606–2610, Mar. 2020.
[10] Y. Sung, "A printed wide-slot antenna with a modified L-shaped microstrip line for wideband applications," *IEEE Trans. Antennas Propag.*, vol. 59, no. 10, pp. 3918–3922, Oct. 2011.
[11] G. A. Casula, P. Maxia, G. Montisci, G. Mazzarella, and F. Gaudiomonte, "A printed LPDA fed by a coplanar waveguide for broadband applications," *IEEE Antennas Wireless Propag. Lett.*, vol. 12, pp. 1232–1235, 2013.
[12] A. Liu and J. Lu, "A UHF deployable log periodic dipole antenna: Concept, design, and experiment," *IEEE Trans. Antennas Propag.*, vol. 69, no. 1, pp. 538–543, Jan. 2021.
[13] P. Fei, Y.-C. Jiao, W. Hu, and F.-S. Zhang, "A miniaturized antipodal Vivaldi antenna with improved radiation characteristics," *IEEE Antennas Wireless Propag. Lett.*, vol. 10, pp. 127–130, 2011.
[14] Y. Liu, W. Zhou, S. Yang, W. Li, P. Li, and S. Yang, "A novel miniaturized Vivaldi antenna using tapered slot edge with resonant cavity structure for ultrawideband applications," *IEEE Antennas Wireless Propag. Lett.*, vol. 15, pp. 1881–1884, 2016.
[15] S. Mukherjee, A. Biswas, and K. V. Srivastava, "Broadband substrate integrated waveguide cavity-backed bow-tie slot antenna," *IEEE Antennas Wireless Propag. Lett.*, vol. 13, pp. 1152–1155, 2014.
[16] J. Cho, T. H. Lim, Y. Kim, and H. Choo, "Design of a wideband printed patch dipole antenna with a balanced on-board feeding network," *J. Electromagn. Eng. Sci.*, vol. 22, no. 6, pp. 631–637, Nov. 2022.
[17] X. Ren, S. Liao, and Q. Xue, "Design of wideband circularly polarized Vivaldi antenna with stable radiation pattern," *IEEE Access*, vol. 6, pp. 637–644, 2018.
[18] G. H. Jeon, P. A. Dzagbletey, and J. Y. Chung, "A cross-joint Vivaldi antenna pair for dual-pol and broadband testing capabilites," *J. Electromagn. Eng. Sci.*, vol. 21, no. 3, pp. 201–209, Jul. 2021.
[19] T. H. Lim, S. Park, C. S. Lee, J.-R. Park, and H. Choo, "A broadband dual-slant polarized metal Vivaldi antenna for a high-power jammer," in *Proc. Int. Symp. Antennas Propag. (ISAP)*, Osaka, Japan, Jan. 2021, pp. 486–495.
[20] *CST Studio Suite: Electromagnetic Field Simulation Software*. [Online]. Available: http://www.cst.com
[21] *Ansoft Coporation HFSS*. [Online]. Available: http://www.an-soft.com/products/hf/hfss/
[22] D. M. Pozar, "Analysis of an infinite phased array of aperture coupled microstrip patches," *IEEE Trans. Antennas Propag.*, vol. 37, no. 4, pp. 418–425, Apr. 1989.
[23] E. Magill and H. Wheeler, "Wide-angle impedance matching of a planar array antenna by a dielectric sheet," *IEEE Trans. Antennas Propag.*, vol. AP-14, no. 1, pp. 49–53, Jan. 1966.
[24] M. Ebrahimpouri, L. F. Herran, and O. Quevedo-Teruel, "Wide-angle impedance matching using glide-symmetric metasurfaces," *IEEE Microw. Wireless Compon. Lett.*, vol. 30, no. 1, pp. 8–11, Jan. 2020.
[25] J. Yun, D. Park, D. Jang, and K. C. Hwang, "Design of an active beam-steering array with a perforated wide-angle impedance matching layer," *IEEE Trans. Antennas Propag.*, vol. 69, no. 9, pp. 6028–6033, Sep. 2021.
[26] B. Zhang and H. Zirath, "A metallic 3-D printed E-band radio front end," *IEEE Microw. Wireless Compon. Lett.*, vol. 26, no. 5, pp. 331–333, May 2016.
[27] D. M. Pozar, "A relation between the active input impedance and the active element pattern of a phased array," *IEEE Trans. Antennas Propag.*, vol. 51, no. 9, pp. 2486–2489, Sep. 2003.
[28] C.-H. Liang, L. Li, and X.-J. Dang, "Inequailty condition for grating lobes of planar phased array," *Prog. Electromagn. Res. B*, vol. 4, pp. 101–113, 2008.
[29] D. F. Kelley and W. L. Stutzman, "Array antenna pattern modeling methods that include mutual coupling effects," *IEEE Trans. Antennas Propag.*, vol. 41, no. 12, pp. 1625–1632, Dec. 1993.
[30] S. Zhang, S. Gong, Q. Gong, Y. Guan, and B. Lu, "Application of the active element pattern method for calculation of the scattering pattern of large finite arrays," *IEEE Antennas Wireless Propag. Lett.*, vol. 10, pp. 83–86, 2011.

SUNGSIK OHM received the B.S. degree in electronic and electrical engineering from Hongik University, Seoul, South Korea, in 2020, where he is currently pursuing the M.S. degree in electronic and electrical engineering. His research interests include jamming systems, array antennas, wireless power transfer systems, wave propagation, and direction finding.

EUNJUNG KANG received the B.S. degree in electronic and electrical engineering from Hongik University, Sejong, South Korea, in 2016, and the M.S. degree in electronic and electrical engineering from Hongik University, Seoul, South Korea, in 2020, where she is currently pursuing the Ph.D. degree in electronic and electrical engineering. She was a Research Engineer with the Korea Electronics Technology Institute (KETI), Seongnam, South Korea, from 2016 to 2017. Her research interests include array antenna for electronic warfare, wireless power transfer systems, LEO satellite electromagnetic wave propagation, direction finding, and GPS antennas.

TAE HEUNG LIM received the B.S., M.S., and Ph.D. degrees in electronic and electrical engineering from Hongik University, Seoul, South Korea, in 2016, 2018, and 2022, respectively. He was a Postdoctoral Researcher with the Ulsan National Institute of Science and Technology (UNIST), in 2022. He is currently a Senior Researcher with the Agency for Defense Development, Daejeon, South Korea. His research interests include sea-based radar, mmWave and sub-THz metasurfaces, high power jamming array antennas, 5G system antennas, time-modulated array, adaptive beamforming, and wave propagations for radar applications.

HOSUNG CHOO (Senior Member, IEEE) received the B.S. degree in radio science and engineering from Hanyang University, Seoul, South Korea, in 1998, and the M.S. and Ph.D. degrees in electrical and computer engineering from the University of Texas at Austin, in 2000 and 2003, respectively. In September 2003, he joined the School of Electronic and Electrical Engineering, Hongik University, Seoul, where he is currently a Professor. His research interests include electrically small antennas for wireless communications, reader and tag antenna for RFID, on-glass and conformal antennas for vehicles and aircraft, and array antenna for GPS applications.